Ultra-Thin Glass Hybrid Cutting by Ultrashort Pulsed Laser Robot

Yongting Yang*[1], Daniel Franz[1], Cemal Esen[2], and Ralf Hellmann[1]

[1]*Applied Laser and Photonics Group, University of Applied Sciences Aschaffenburg, Würzburger Straße 45, Aschaffenburg, 63743, Bavaria, Germany*
[2]*Applied Laser Technologies, Ruhr University Bochum, Universitätsstraße 150, Bochum, 44801, Nordrhein-Westfalen, Germany*
**Corresponding author's e-mail: Yongting.Yang@th-ab.de*

We report on a hybrid cutting method of ultra-thin glass cutting using an ultrashort pulsed laser robot system. An ultrashort pulsed laser is fixed on the elongation of one axis of a six-axes articulated industrial robot. The laser beam is guided by mirrors along the robot axes into a 2D galvanometer scanner with a telecentric F-Theta lens, the latter being fixed on the last robot axis. The system due to its high flexibility expands ultrashort pulsed laser processing to a large-scale area micromachining toll with true three-dimension capabilities. Furthermore, the combined movement of scanner and robot, here specifically referred to as hybrid cutting movement, extends the system's overall processing abilities. In an experimental study of cutting ultra-thin glass D263, scanner speed as well as laser pulse duration are varied for a continuous robot movement speed at 20 mm·s^{-1}. The quality of the ultra-thin glass cutting is evaluated in terms of minimal glass chipping and maximum flexural strength of the cut specimen. Applying a three-line scan trajectory, both quality aspects are found to be optimized for a pulse duration of 7 ps and the scan speed of 700 mm·s^{-1}. To highlight the potential of this new hybrid and true 3D ultra-thin glass cutting, a rectangular is cut from a bent glass sample.

DOI: 10.2961/jlmn.2025.02.2011
Keywords: ultrashort pulsed laser robot, laser robot, ultra-thin glass cutting, glass bending test

1. Introduction

Besides its fundamentally peculiar physical and chemical properties, ultra-thin glass (UTG) exhibits excellent bending capabilities [1], making it the ultimate choice for glass applications in modern display technologies [2], flexible electronics [3], photovoltaic [4, 5] and biomedical applications [6].

However, at the same time UTG is highly sensitive towards the generation of residual stress or even breakage under most processing technologies, posing challenges on manufacturing and demanding innovative micromachining approaches. For example, in conventional mechanical processing, glass is scribed using a diamond tip or wheel cutter and then broken by external force [7]. Due to the scribing mechanism, the crack cannot be completely avoided [8]. Additional processes such as grinding and polishing are required to achieve the desired cutting-edge quality and strength [9]. However, problems such as large grooves and chipping, however, result in high residual stress and reduced bending strength.

Therefore, nowadays lasers, as a contactless high precision processing technology, are widely used in glass cutting [10]. CO_2 lasers have been applied for glass thermal cutting. Mishra et al. [11] optimized cutting parameters of a sealed CO_2 laser and cut through a 75 µm borosilicate glass with multilayer thin films at both sides. Itoh et al. [12] combined a CO_2 laser with the 150 µm beam diameter with an elliptical beam of a larger geometry for 100 µm thin glass cutting. The process reduced the residual thermal stress in material and achieved a maximum flexural strength of 520 MPa.

Ultrashort pulsed (USP) lasers with a pulse duration that is shorter than the thermal conduction timescale, minimize the thermal effect during the process. Nonlinear interaction mechanisms such as multiphoton absorption and avalanche ionization enhance the strength of USP laser for the glass processing. The common USP laser based thin glass cutting process is laser scribing and bending. Bessel-beams as an approximation of a non-diffracting beam improves the intensity distribution along the propagation [13], which has been applied for UTG scribing. Shin et al. [14] compared the influence of the modification interval and the relative position of the focal plane as well as the pulse energy of the Bessel beam for the UTG internal modification, arriving a maximum strength of 370 MPa. Luo et al. [15] developed a laser composite processing method, in which 300 µm glass was internally modified by focusing a 2 µm laser in the middle of the glass, followed by the scribing process with moving the laser focus on the surface. The glass was separated by mechanical bending and the strength of 369 MPa was achieved by the optimal parameter.

Furthermore, UTG is able to be cut by USP laser directly by ablation using a galvanometer. In Ref. 16, 1.5 mm circles were cut out from the 50 µm and 100 µm thick glass by a picosecond laser, where the movement of galvanometer scanner were planted along a spiral track for avoiding overheating and cracks generated by excessive thermal stress. Additionally, borosilicate glass with a thickness of 110 µm was cut though by ablation in ambient air and water, in

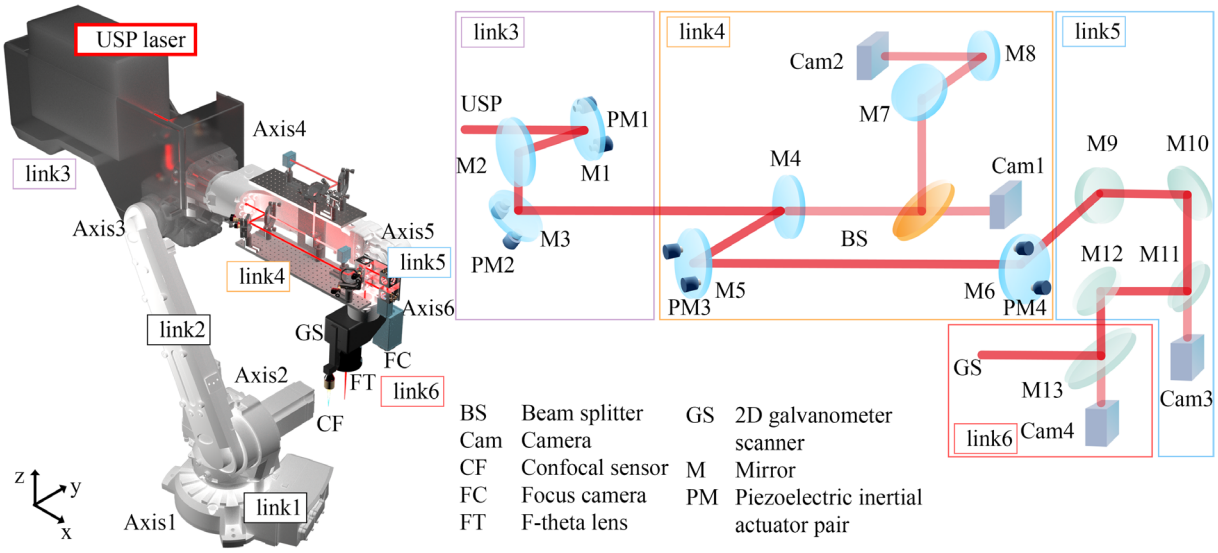

Fig. 1 Illustration of USPLR system and beam guidance within the setup. A USP laser is fixed on the Link3. The laser beam is guided by mirrors across several axes and arriving to the 2D galvanometer scanner with F-Theta lens mounted on the Link6. Mirrors with piezoelectric inertial actuator pairs and cameras are used for beam position stabilization.

which a similar cutting quality was observed in both cutting environments [17]. Bottom-up cutting due to the reduced damage threshold has been used for glass cutting [18, 19]. The 100 µm thin glass was cut applying a high numerical aperture objective. Unexpected back-surface ablation was avoided by the bottom-up cutting and resulted in an increase in edge strength for both sides. The maximum edge strength on the back side was 65% higher than the edge cut by the conventional top-down process [20].

However, based on the traditional beam delivery systems and conventional relative movement between the laser beam and the workpiece, existing UTG cutting processes are limited in their geometry and to 2-2.5D workpiece geometries. Recently, an ultrashort pulsed laser robot (USPLR) system was developed and discussed in our previous research [21, 22]. The laser is guided by optical components along the robot axes arriving at a 2D galvanometer scanner and a F-Theta lens for the material processing. By combining the strength of USP laser and the high flexibility of a six axes robot, this system expands USP laser processing into a large processing dimension and into a true 3D machining approach. 100 µm thin glass was cut through by this system without showing any cracks, in an approach in which the scanner is moved along the designed track after the robot has arrived on the position [21]. This motivates the application of the system in large-scale UTG processing. Additionally, the simultaneous scanner movement and robot movement (hybrid movement) enhances the system flexibility compared to the conventional galvanometer scanner cutting, which shows a potential for improving the UTG processing capabilities of USPLR system.

This contribution aims to utilize the USPLR system for hybrid cutting of UTG. The hybrid cutting approach is compared with the standard cutting. A comprehensive experimental study of the cutting edge quality considering various scanner speeds and laser pulse durations is presented. A three-point bending test is applied to determine the optimal parameters. Last but not least, an example of hybrid cutting for 3D UTG processing is demonstrated to highlight the systems capabilities.

2. Experimental setup

As illustrated in Fig. 1, a 1030 nm USP laser (CB3-40W, Light Conversion) is mounted between Axis3 and Axis4 of a six-axis articulated industrial robot (IRB 2600ID-8/2.00, ABB). The processing unit located on the end of Link6 consists of two 2D galvanometer deflectors (RTAX-A15 and RT AY-A15, Newson) and a telecentric F-theta lens with a focal length of 160 mm (JENar Silverline F-Theta, Jenoptik). The laser beam is guided by mirrors, propagating along the subsequent robot axes to the processing unit. In addition, a cascaded beam stabilization system integrated between Link3 to Link6 ensures a high overlap of the current beam propagation axis to the optimal optical alignment crossing axes during the processing. Each stage consists of two mirrors aligned by a piezoelectrical inertial actuator (PIAK10, Thorlabs) pair and two cameras for the current beam position detection, where M1, M2, Cam1 and Cam2 (2x DMK 37AUX250, The Imaging Source) are used for the first stage, M5, M6, Cam3 and Cam4 (2x DMK 38UX541, The Imaging Source) contribute to the beam misalignment correction

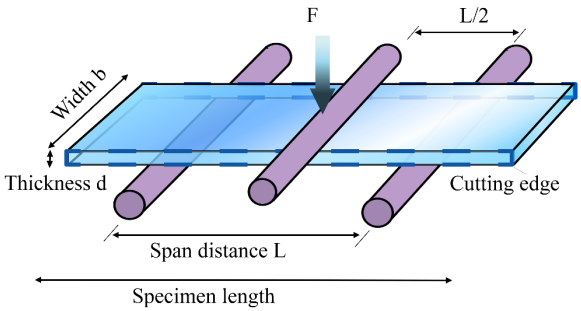

Fig. 2 Three-point bending test for the UTG. The specimen has 100 mm in length and 10 mm in width, with both 100 mm sides cut using various cutting parameters.

of second stage (for more details see [23]). A confocal sensor and a focus camera with zoom adjustment function (DMK 39GX548-Z20, The Imaging Source) are applied for the beam focus monitoring before and during the process with a complex system movement.

Borosilicate ultra-thin glass (D263, Schott) with the dimension of 440 mm×360 mm×100 µm was initially cut into pieces (measuring 15 mm×180 mm×100 µm) by the USPLR system for the subsequent hybrid cutting. Theses glass substrates were then further processed under various hybrid cutting parameters to produce final specimens measuring 15 mm×20 mm×100 µm, with the 20 mm edges cut using the hybrid cutting parameters. The laser applied in these experiments exhibits a spot diameter of 64 µm ($1/e^2$) and a repetition rate of 200 kHz. Circular polarization was applied to avoid the influence of polarization on cutting quality. A laser scanning microscope (LSM, VK-X3000, Keyence) was used to record images. The definitions of crack and chip follow those reported by reported by Markauskas et. al. [17] (see Fig. 3(a)).

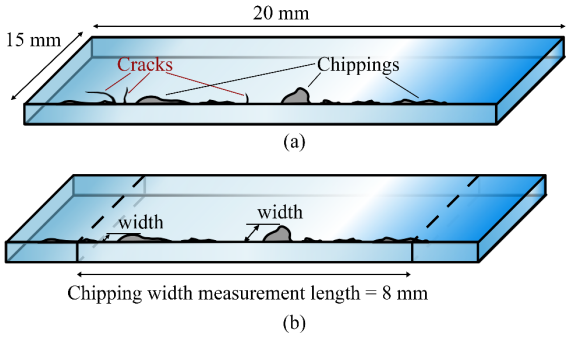

Fig. 3 Illustration of cutting edge. (a) Definition of cracks and chippings on the cutting edge. (b) The chipping width for the crack-free cutting edges are measured crossing 8 mm.

The cutting quality of all crack-free edges was evaluated according to the method introduced in [17]. The width of chipping was used as the criterion for assessing cutting edge quality (Fig. 3(b)). Due to the high sensitivity of UTG, the average and maximum width of chipping was measured across an 8 mm cutting length. A z-score method for outline detection was applied additionally. The z-score of individual measured width was calculated with:

$$z_i = \frac{X_i - \mu}{s}, \qquad (1)$$

where X_i is individual width data, µ is the mean of total measured width and s is the standard deviation of the total measured data. Defining the width with the z-score over 1.96·s as outliers.

To compare the flexural strength of the parameters generating a crack-free cutting edge, a three-point bending test (EZ Test, Shimadzu) was applied in the experiment. Specimens with dimensions of 100 mm×10 mm were cut using the USPLR system, with the 100 mm edge cut under various hybrid cutting parameters. The support span distance L was set at 70 mm and the loading rate was 5 mm·min^{-1} (see Fig. 2). The flexural strength, denoted by σ, is calculated using equation (1):

$$\sigma = \frac{3FL}{2bd^2}, \qquad (2)$$

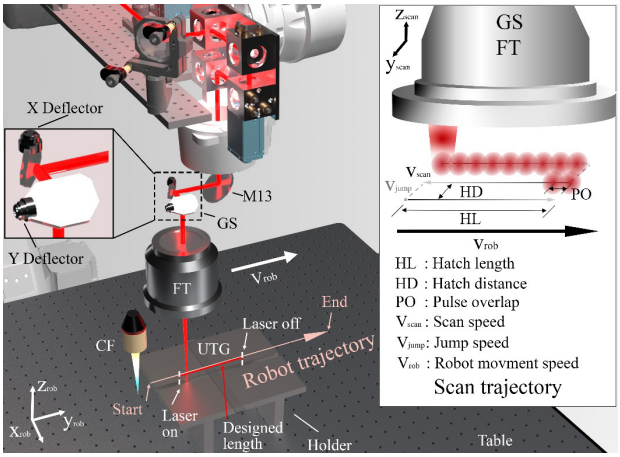

Fig. 4 Illustration of hybrid cutting process using the USPLR system. Robot moves along the robot trajectory with the speed V_{rob}. Two deflectors align laser beam in the x and y direction. The deflectors move along the scan trajectory with a defined pulse overlap PO and distance HD repeatedly, during the robot movement. The robot trajectory and direction shown in the illustration are used in all experiments discussed in Section 4. The scan trajectory shown in the inset is applied to all hybrid cutting experiments discussed in subsequent sections.

where the F is the maximum load, b is the specimen width, and d is the specimen thickness [24, 25].

3. Cutting methods using the USPLR system

For standard cutting using the USPLR system, the robot follows a predefined robot trajectory while the laser is activated, and no scanner movement occurs during the robot motion.

The hybrid cutting using the USPLR system is illustrated in Fig. 4. Since the defocusing of laser beam leads to an increase in beam diameter, in turn resulting in a decrease in fluences, the UTG specimen is placed on a holder to ensure the correct beam focus during the process. The low thickness and high transmission of the UTG necessitates a gap between the holder, which avoids the influence of reflection and wrong absorption of the holder instance. To ensure the cutting performance, a minimum distance of 60 mm is required between the cutting plane and the table.

The movement trajectory is defined separately for the robot and the scanner. In each cutting process, the robot moves along the trajectory in the processing area with the speed V_{rob} for one time (Robot trajectory). Two galvanometer deflectors align the laser beam in the x and y direction (X Deflector, Y Deflector) along the designed hatch lines with the scan speed V_{scan} and jump speed V_{jump}, respectively, maintaining a constant pulse overlap along the scan direction and a constant hatch line distance (illustrated in the inset of Fig. 4). The acceleration and deceleration of the robot induce, with respect to micromachining, significant vibrations of the system, which reduce the cutting quality. To avoid these effects, the laser is activated behind the start of robot movement and deactivated before the end of the robot movement. During the activated-laser time duration, the scanner continuously repeats the scan trajectory. The start and end offset are determined based on the robot speed, so that the laser is activated at the beginning of the design length and deactivated at the end of the design length. In this contribution, the beam focus

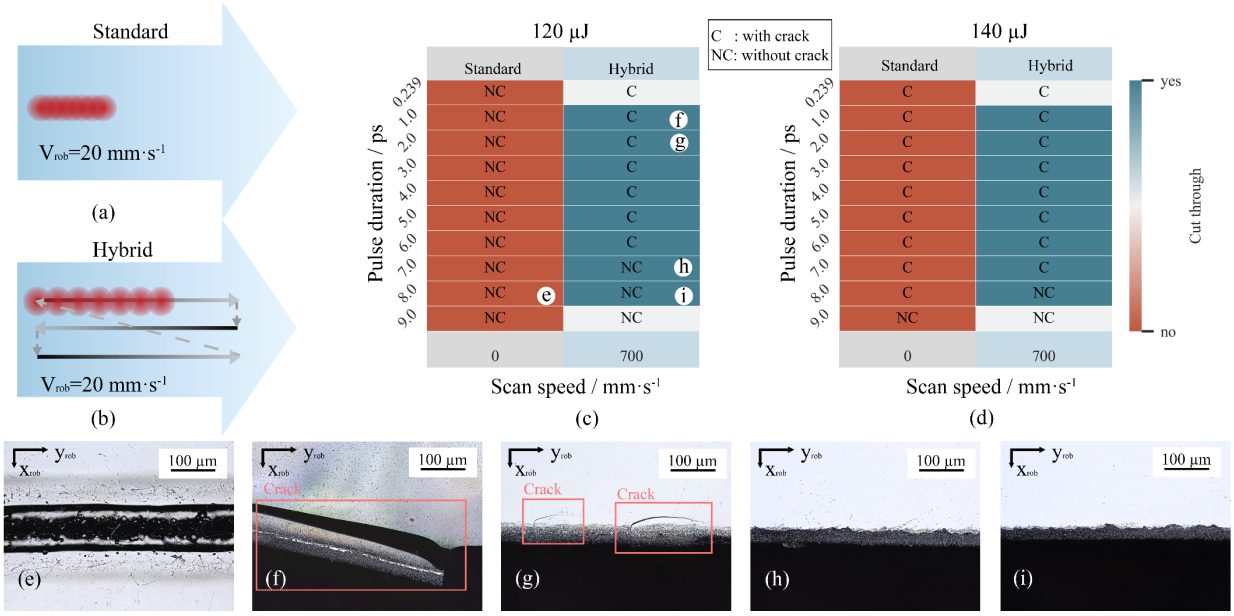

Fig. 5 Standard cutting and hybrid cutting using USPLR system. The robot speed is 20 mm·s^{-1}. During the robot movement (a) the laser is activated in the standard cutting without scanner movement and (b) scanner moves along the scanner trajectory repetitively in the hybrid cutting (solid line for scan direction, dotted line for jump direction). The cutting results are compared for (c) 120 µJ and (d) 140 µJ. (e) shows an incompletely cut, (f, g) show a cutting edge with cracks, and (h, i) highlight crack-free cutting edges. The applied parameters for (e-i) are shown in (c). Please note that, for the appearance of large crack, the cutting edge shown in (f) was rotated, and the surface was not cleaned.

was set on the processing surface and adjusted using a confocal sensor before the process begins.

4. Results and discussion

4.1 Standard cutting and hybrid cutting

The USPLR system exhibits stable movement with a low vibration during acceleration and deceleration process at the robot speed of 20 mm·s^{-1}, which therefore was used for both cutting methods in this contribution. The robot trajectory length was set as 100 mm, including a start offset of 30 mm. Please note that robot follows the robot trajectory only once in both standard and hybrid cutting methods. A pulse duration from 0.239 to 9 ps as well as pulse energies of 120 µJ and 140 µJ (corresponding to peak fluences of 7.46 J/cm^2 and 8.70 J/cm^2, respectively), were compared for both methods. The standard and hybrid cutting processes are illustrated in Fig. 5(a) and Fig. 5(b). For hybrid cutting, the scan trajectory consists of three hatch lines with HD = 16 µm and HL = 4 mm. The scan speed is 700 mm·s^{-1} and the jump speed is 1000 mm·s^{-1}. Since the pulse overlap along the scan lines differs from the pulse overlap between scan lines and robot moves continuously, a bi-directional scan was applied to reduce an inhomogeneous energy distribution across the entire cutting trajectory.

The results are summarized in Fig. 5(c-d). Cracks were frequently observed at higher pulse energies for both cutting methods. In the hybrid cutting, the glass was cut through with cracks within the 0.239 to 7 ps pulse duration range using 140 µJ, whereas a crack-free cut edge was achieved between 7 ps and 8 ps when using 120 µJ. Notably, a high pulse energy induces high thermal stresses and leads to the crack formation [16]. Please note that, the 100 µm UTG could not be fully cut through using standard cutting across the entire pulse duration range for both pulse energies. The ablation depth increases with a higher number of laser passes, while maintaining constant pulse energy [16, 26]. In turn, the applied pulse energy is too low to cut through the 100 µm glass in the standard cutting method. In contract to standard cutting, the UTG was cut through successfully using the hybrid cutting approach in the picosecond pulse regime. The specimen was semi-cut-through with the pulse duration of 239 fs and 9 ps, meaning the glass did not separate immediately after process but fractured due to a slight external force such as touching or handling during transport. The scan movement along the robot movement direction reduces the pulse overlap at each pass, leading to a lower residual heat in the material. Simultaneously, the movement of laser spot before and behind the base position realizes a comparable multi-passes along the cutting trajectory. This avoids the buildup of extremely high temperature in the processing volume and suppresses crack formation [27].

The cutting edges produced by both methods are illustrated in Fig. 5(e-f). The glass was not fully cut through using standard cutting (in Fig. 5(e)). In the hybrid process, cracks appeared on the cutting edge using the pulse duration of 1 ps and 2 ps (Fig. 5(f, g)), while a crack-free cutting edge was observed at 7 ps and 8 ps (Fig. 5(h-i)). One assumption is the damage threshold increases at longer pulse durations [28]. Additionally, no significant morphological difference on the cutting edge was observed by microscopy at 7 ps and 8 ps in the hybrid cutting. Overall, the movement of the scanner enhances processing capability in comparison to the standard cutting.

4.2 Impact of scan speed on UTG hybrid cutting performance

Based on the cutting results in Fig. 5, scan speeds ranging from 300 mm·s^{-1} to 900 mm·s^{-1} were compared for the pulse durations between 6 ps and 8 ps at the pulse energy of

Table 1 Comparison of mean and maximum chipping width of crack-free cutting edges.

Scan speed / mm·s^{-1}	Max. / µm		Max. Outlier / µm		Mean / µm	
Pulse duration / ps	7	8	7	8	7	8
600		**17.80**		**39.58**		5.74
700	13.24	17.07	19.68	27.07	5.34	**8.77**
800	16.80		39.06		7.26	

120 µJ, while remaining the same scan trajectory, jump speed as well as robot speed applied in section 4.1.

The cutting result is shown in Fig. 6(a). Cracks were observed for all pulse durations when using scan speeds below 600 mm·s^{-1}. Here, the time interval between two subsequent pulses is shorter than the thermal diffusion time of borosilicate glass (~10 µs [29]) at the repetition rate of 200 kHz, causing heat accumulation that contributed to the process. However, the extremely high pulse overlap nonetheless induces thermal damage and leads to crack formation [27], as shown in Fig. 6(b). Pulse overlap decreases with increasing scan speed, which prevents excessive temperature buildup in the processing region. No cracks appeared at the scan speeds higher than 800 mm·s^{-1}. However, the low accumulated pulse energies at high speeds resulted in semi-cut-through edges. In addition, the scan speed required for crack-free cutting edges decreases at long pulse durations. The crack-free cutting edge pretended firstly at 600 mm·s^{-1} using the pulse duration of 8 ps, while the minimum scan speed for crack-free edges was 700 mm·s^{-1} for the pulse duration of 7 ps.

As shown in Fig. 5(h, i) and Fig. 6(c), chipping is observed on the crack-free cutting edges. The mean and maximum chipping width as well as the maximum width of outliers are shown in Table. 1. The mean chipping width increases at high scan speeds for both pulse durations. The minimum mean chipping width of 5.34 µm is observed at 700 mm·s^{-1} with the pulse duration of 7 ps. A slightly higher mean chipping width is shown at the scan speed of 600 mm·s^{-1}and the pulse duration of 8 ps. Notably, lower maximum chipping widths are observed at 700 mm·s^{-1} for both pulse durations. The maximum chipping width at 700 mm·s^{-1} and 7 ps is 13.24 µm, which is approximately 21% lower than the width at 800 mm·s^{-1}. The maximum

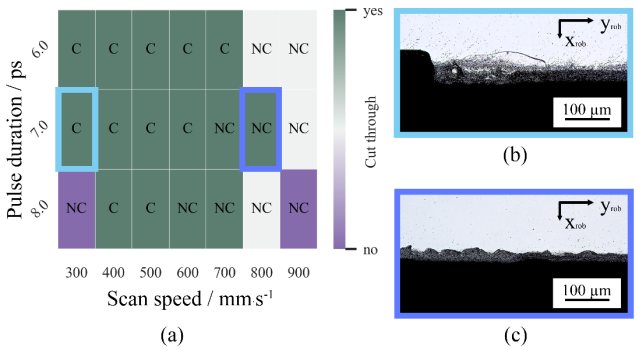

Fig. 6 Influence of scan speed and pulse duration on the cutting edge. (a) Processing range. NC: no crack, C: crack. (b) Cutting edge at 7 ps with scan speed of 300 mm·s^{-1}. (c) Cutting edge at 7 ps with scan speed of 800 mm·s^{-1}.

width for outliers at this speed is half of the width at 800 mm·s^{-1}.

A three-point bending test was applied to evaluate and compare the cutting quality in the scan speed range of 500 mm·s^{-1} to 800 mm·s^{-1} at the pulse duration of 7 ps and 8 ps, while maintaining the pulse energy of 120 µJ (in Fig. 7). Please note that the same scan trajectory, jump speed as well as robot speed applied in section 4.1 were used for the test specimen fabrication. On the one hand, a beam defocusing could not be completely avoided during the movement crossing large area due to the system structure. On the other hand, glass processing is sensitive to the deviations in the processing condition considering the glass producing tech-

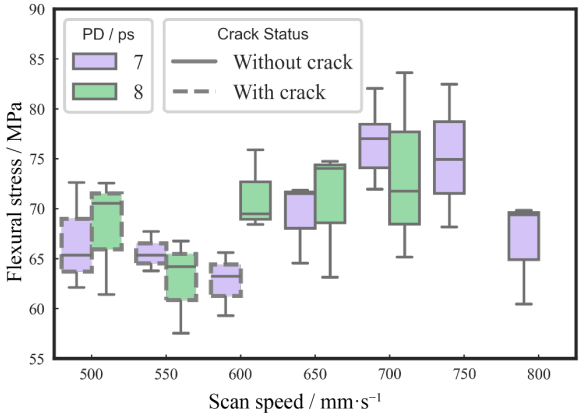

Fig. 7 Three-point bending test for the scan speeds from 500 mm·s^{-1} to 800 mm·s^{-1}. The line in the box indicates the median value. Please note that the large specimen was not completely cut through at 750 mm·s^{-1} and 800 mm·s^{-1}, 8 ps. Please note that PD is pulse duration.

nology. For example, the acceptable beam focus offset range decreases because low pulse overlaps. To minimize the influence of variations, three specimens were processed for each parameter. Cracks appeared at low scan speeds for both pulse durations. A minimum scan speed of 600 mm·s^{-1} is required for a crack-free cutting at 8 ps, while a speed of 650 mm·s^{-1} for 7 ps. Cracks reduce the flexural stress significantly, the flexural stress of the crack-free cutting edge is 9.8% higher than the edge with crack at 600 mm·s^{-1}. The maximum median stress of 76.33 MPa for all crack-free cutting edges is achieved at 700 mm·s^{-1} and 7 ps, where a lower mean chipping width is observed (in Table 1). A high maximum chipping width not only contributes to reduced flexural strength but also increases the deviation of processing quality. At the pulse duration of 7 ps, a high chipping width observed at 800 mm·s^{-1} leads to a decrease in flexural stress as compared to the value at 700 mm·s^{-1}. The maximum stress deviation is shown at the speed of 750 mm·s^{-1}. The same

trend is noted at 8 ps, where a lower deviation is shown at 600 mm·s^{-1} compared to the value at 700 mm·s^{-1}. The higher deviation shown for the 8 ps is attributed to the increased chipping width compared to the 7 ps at the scan speed of 700 mm·s^{-1}. Compared to 8 ps, a broader processing range is achieved using the pulse duration of 7 ps. A lower average chipping width combined with a low maximum chipping width contributes to higher flexural stress, indicating improving the cutting quality.

4.3 Demonstration of real 3D hybrid cutting

Apparently, hybrid cutting reduces the heat induced stress in the material compared to the standard cutting process using USPLR system. The movement of the deflectors enlarged the acceptable beam focus offset range compared to the standard cutting. These realize a real 3D cutting of ultra-thin glass.

The 3D processing of UTG is exemplified in Fig. 8(a-c). A 167 mm×26 mm glass specimen was cut out from a large glass substrate by the USPLR system using 2D hybrid cutting method. The specimen then is bent and clamped between two holders with the distance of 163.2 mm, resulting in a radius of 225.2 mm. A 90 mm×5 mm rectangle is designed for the real 3D hybrid cutting. The robot trajectory is defined to follow the curved surface of the specimen, ensuring that the laser propagation axis after the F-Theta lens remains parallel to the surface normal along the entire trajectory. The highest position of surface is determined by confocal sensor, the translation and rotation of the TCP at this position is loaded from robot controller. Three points are required for a curve trajectory in robot control. The start, center and end points of robot trajectory are calculated using the measured specimen length and holder distance, the defined robot speed, the specified cutting length, and the top point coordinates. Each point consists of translation and rotation information.

During the robot movement, the deflectors start the movement as soon as the robot reaches the start position of designed length and then follow the defined scanner trajectory repetitively until the robot arrives at the end position (Fig. 8(a-c)). The scanner trajectory introduced in section 4.1 as well as the pulse duration of 7 ps and the scan speed of 700 mm·s^{-1} were applied in the 3D cutting. The robot speed was 20 mm·s^{-1} along the surface. Fig. 8(d-f) shows the processed UTG sample. A rectangle was cut from the UTG sample, with both long edges processed using the hybrid cutting method. The short edges were cut by deflector movement along, after the system positioned the laser beam at the respective locations. The hybrid cutting in 3D results a cutting edge without cracks, which is comparable to the cutting edge shown in the Ref. [7].

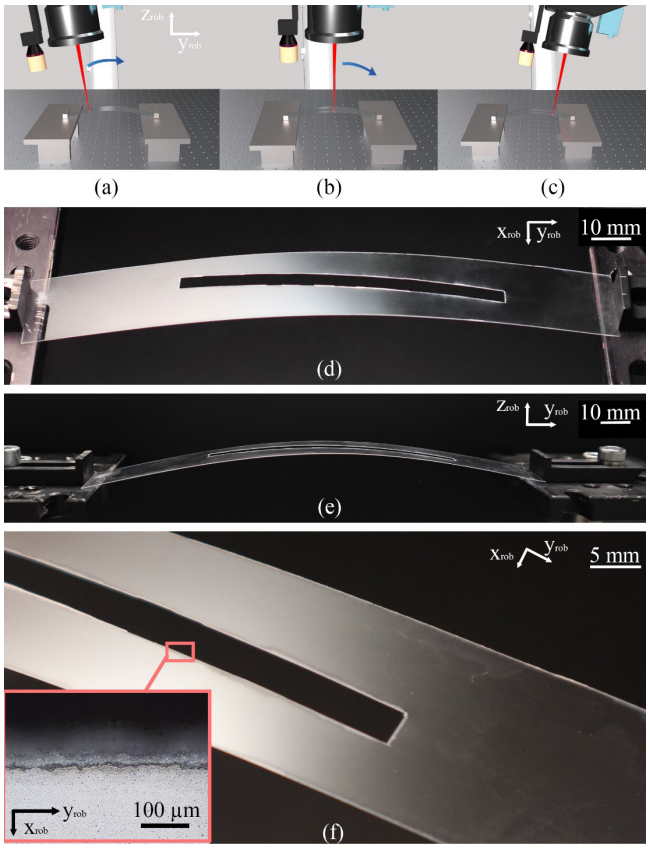

Fig. 8 Image of the excellent 3D UTG processing results with the USPLR system. (a) The glass sample is bent and clamped between two holders. System aligns the scanner and F-Theta lens orientation to the surface normal direction at the start position. (b) The system moves along the curved surface, maintaining the beam focus position on the surface and the beam propagating axis behind F-Theta lens remains parallel to the normal of surface. The deflectors follow the scanner trajectory repetitively during the robot movement. (c) The laser is deactivated as the system reaches the end position. The processed glass sample in (d) top, (e) side, (f) detailed view, the microscopic image of the cutting edge is shown in the inset for better visualization.

5. Conclusion

A cutting method combining scanner and robot movement was developed on an ultrashort pulsed laser robot system. A scanner fixed at the end of the last axis of the robot enhances the flexibility of the entire laser optic system. The robot motion along a robot trajectory and the bi-directional movement of the scanner along a scan trajectory during the robot movement, denoted as hybrid movement, was applied for ultra-thin glass cutting. Under identical robot speeds and pulse energies, the hybrid movement successfully achieved full-through cutting of the ultra-thin glass, while the standard cutting method failed. Crack-free cutting edges were observed using the pulse duration of 7 ps and 8 ps, where the maximum median flexural stress of 76 MPa was achieved using the scan speed of 700 mm·s^{-1} and a pulse duration of 7 ps. To highlight the unique potential of the hybrid cutting approach, it was applied to real 3D ultra-thin glass cutting crossing a large area, in which a rectangle was cut from the bent glass sample.

Particularly, the scanner movement improves the flexibility of the system and expands the processing capabilities of the ultrashort pulsed laser robot system. The successful realization of both 2D and 3D cutting of ultra-thin glass demonstrates the system's suitability for precision processing and highlights its potential as an alternative to standard laser machines for industrial applications.

Acknowledgments

This research was funded by the Bavarian Ministry of State for Economy, Land Development and Energy (project

RoboSens, grant number DIK0375/01) and by the Bavarian Ministry of Science and Arts (project LEZ, grant number H.2-F1116.AS/34/2).

References

[1] A. Plichta, A. Weber, and A. Habeck: MRS Proc., 769, (2003) 91.
[2] M.-H. Ha, J.-K. Choi, B.-M. Park, and K.-Y. Han: J. Mech. Sci. Technol., 35, (2021) 661.
[3] G. C. Righini, J. Krzak, A. Lukowiak, G. Macrelli, S. Varas, and M. Ferrari: Opt. Mater., 115, (2021) 111011.
[4] J. Dziedzic and M. Inglot: Acta Phys. Pol. A, 132, (2017) 176.
[5] S. Kim, H. van Quy, and C. W. Bark: Mater. Today Energy, 19, (2021) 100583.
[6] Y. Yalikun, N. Tanaka, Y. Hosokawa, T. Iino, and Y. Tanaka: Biomed. Microdevices, 19, (2017) 85.
[7] H. Shin and D. Kim: Opt. Laser Technol., 102, (2018) 1.
[8] D. Li, J. Li, H. Kong, J. Guo, L. Huang, and Y. Liu: Coatings, 15, (2025) 275.
[9] M. P. Jahan, A. Perveen, and A. M. Rumsey: Mach. Sci. Technol., 23, (2019) 264.
[10] S. Nisar, L. Li, and M. A. Sheikh: J. Laser Appl., 25, (2013) 42010.
[11] S. Mishra *et al.*: Opt. Lasers Eng., 90, (2017) 128.
[12] S. Itoh *et al.*: Opt. Laser Technol., 181, (2025) 112004.
[13] O. Brzobohatý, T. Cizmár, and P. Zemánek: Opt. Express, 16, (2008) 12688.
[14] H. Shin and D. Kim: Opt. Laser Technol., 129, (2020) 106307.
[15] Y. Luo, X. Xie, Z. Zhang, Z. Li, and Y. Huang: Opt. Commun., 555, (2024) 130224.
[16] K. L. Wlodarczyk, A. Brunton, P. Rumsby, and D. P. Hand: Opt. Lasers Eng., 78, (2016) 64.
[17] E. Markauskas, L. Zubauskas, G. Račiukaitis, and P. Gečys: Micromachines, 14, (2023) 176.
[18] J. Dudutis *et al.*: Opt. Express, 30, (2022) 4564.
[19] M. Mackevičiūtė, J. Dudutis, and P. Gečys: Opt. Lasers Eng., 183, (2024) 108490.
[20] H. Shin, J. Noh, and D. Kim: Opt. Laser Technol., 138, (2021) 106921.
[21] D. Franz, Y. Yang, L. Michel, C. Esen, and R. Hellmann: J. Laser Appl., 35, (2023) 42057.
[22] Y. Yang, D. Franz, C. Esen, and R. Hellmann: J. Laser Appl., 35, (2023) 42039.
[23] Y. Yang, D. Franz, C. Esen, and R. Hellmann: J. Intell. Manuf., (2025).
[24] S. M. Chung, A. U. J. Yap, S. P. Chandra, and C. T. Lim: J. Biomed. Mater. Res. B Appl. Biomater., 71, (2004) 278.
[25] H. J. Chen, J. H. Yeh, and M. Y. Tsai: 2018 20th International Conference on Electronic Materials and Packaging (EMAP), Clear Water Bay, Hong Kong, (122018) 1.
[26] D. Crimella, T. Jwad, and A. G. Demir: Opt. Laser Technol., 166, (2023) 109645.
[27] M. Sun, U. Eppelt, C. Hartmann, W. Schulz, J. Zhu, and Z. Lin: Opt. Laser Technol., 80, (2016) 227.
[28] M. Sun *et al.:* Laser-Induced Damage in Optical Materials: 2012, Boulder, Colorado, USA, (2012) 853007.
[29] M. Sakakura, M. Terazima, Y. Shimotsuma, K. Miura, and K. Hirao: Opt. Express, 15, (2007) 16800.

(Received: June 5, 2025, Accepted: August 31, 2025)